https://doi.org/10.5194/acp-2022-110
Preprint. Discussion started: 7 April 2022

Atmospheric Chemistry and Physics Discussions

Peculiar COVID-19 effects in the Greater Tokyo Area revealed by spatiotemporal variabilities of tropospheric gases and light-absorbing aerosols

Alessandro Damiani[1], Hitoshi Irie[1], Dmitry Belikov[1], Shuei Kaizuka[1], Hossain Mohammed Syedul Hoque[2], Raul R. Cordero[3]

[1]Center for Environmental Remote Sensing (CEReS), Chiba University, Chiba, 2638522, Japan
[2]Graduate School of Environmental Studies, Nagoya University, Nagoya, 4640064, Japan
[3]Department of Physics, Universidad de Santiago de Chile, Santiago, 3363, Chile

Correspondence to: Alessandro Damiani (alecarlo.damiani@gmail.com)

Abstract. This study investigated the spatiotemporal variabilities in nitrogen dioxide (NO_2), formaldehyde (HCHO), ozone (O_3), and light-absorbing aerosols within the Greater Tokyo Area, Japan, the most populous metropolitan area in the world. The analysis was based on total column, partial column, and in situ observations retrieved from multiple platforms and additional information obtained from reanalysis and box model simulations. This study mainly covers the 2013–2020 period, focusing on 2020, when air quality was influenced by the coronavirus disease 2019 (COVID-19) pandemic. In 2020 overall, NO_2 concentrations were reduced by about 10% annually, with reductions exceeding 40% in some areas during the pandemic state of emergency. Light-absorbing aerosol levels were also reduced for most of 2020, while smaller fluctuations in HCHO and O_3 were observed. Moreover, the degree of weekly cycling of NO_2, HCHO, and light-absorbing aerosol levels was significantly enhanced in urban areas during 2020. The latter changes were unprecedented in recent years and potentially related to coincident reduced mobility in Japan, which, in contrast to other countries, was anomalously low on weekends in 2020. This finding suggests that, despite the lack of strict legal restrictions in Japan, widespread adherence to recommendations designed to limit the spread of the pandemic caused modification of common habits, resulting in unique air quality changes.

1 Introduction

Fossil fuel combustion is the dominant source of nitrogen oxides (NO_x) in the atmosphere, to which traffic is the main contributor, followed by thermal power plants. Other sources include emissions from fires, soils, and lightning. Consequently, NO_x are among the main drivers of air quality degradation in urban areas, and epidemiological studies have shown that nitrogen dioxide (NO_2) exposure is often associated with adverse health effects such as lung cancer, asthma, and cardiopulmonary mortality (e.g., Hamra et al., 2015). Therefore, NO_2 is carefully monitored using both surface and satellite instruments, and is often used as an indicator of air pollution. Moreover, NO_x are precursors to secondary aerosols and catalyze the formation of tropospheric ozone (O_3), with consequences for the climate. Due to its short lifetime on the order of

https://doi.org/10.5194/acp-2022-110
Preprint. Discussion started: 7 April 2022


Atmospheric Chemistry and Physics Discussions

a few hours, NO_2 is an excellent marker for anthropogenic emissions, and satellites often show enhanced NO_2 around large cities and thermal power plants (e.g., Beirle et al., 2003). Therefore, in the past, satellite NO_2 observations have been exploited to evaluate the effectiveness of long-term abatement strategies, the effects of economic recessions, and the impacts of short-term emissions regulations on air quality (e.g., Russell et al., 2012; Lee et al., 2021).

Along with volatile organic compounds (VOCs), NO_x are major O_3 precursors. Nevertheless, in contrast to rural sites where NO_x-limited conditions usually prevail, in urban locations, under VOC-limited (i.e., NO_x-saturated) conditions, a reduction in NO_x is often associated with an increase in O_3 due to reduction of the NO titration effect (Murphy et al., 2007). Indeed, in recent years, emissions of O_3 precursors have significantly decreased worldwide (Russell et al., 2012; Geddes et al., 2016; Georgoulias et al., 2019), while tropospheric ozone has increased (Ziemke et al., 2019; Li et al., 2019; Lee et al., 2021). This general tendency has been confirmed in Japan (e.g., Akimoto, 2017) and, recently, in the Kanto region, where both NO_2 and formaldehyde (HCHO) (as a proxy for non-methane VOC, NMVOC) were reduced and O_3 recovered slightly during the period of 2013–2019 (Irie et al., 2021).

Due to their association with human activities, anthropogenic NO_x emissions often display a weekly cycle. The term 'weekend effect' refers to the difference in pollutant concentrations between weekdays and weekends (e.g., Cleveland et al., 1974). In the same manner, emissions usually decrease during holiday periods, and an equivalent 'holiday effect' can be defined (e.g., Tan et al., 2009). Reduced NO_x levels on rest days are often coupled with increased O_3 in and around cities (Cleveland et al., 1974; Murphy et al., 2007) but not in rural areas (Sicard et al., 2020a). The weekly cycles of both NO_2 and O_3 have been extensively investigated in previous research using both ground-level (Cleveland et al., 1974; Sadanaga et al., 2012; Zou et al., 2019; Sicard et al., 2020a) and satellite (Beirle et al., 2003; Stavrakou et al., 2020) observations. A satellite-based analysis of the global temporal evolution of the NO_2 weekly cycle showed that it has become smaller in recent years (Stavrakou et al., 2020). This trend has been explained by the current reduction in NO_x emissions, confounding of anthropogenic and background NO_x, and secondarily, by an increase in NO_2 lifetime. On the other hand, a recent study of the O_3 weekend effect revealed a significant downward trend (Sicard et al., 2020a). Overall, analysis of the response of O_3 formation to emission changes supports the development of strategies to reduce precursor emissions and improve air quality.

The lockdowns caused by the coronavirus disease 2019 (COVID-19) pandemic represent an opportunity to assess the impacts of human activities on the environment and human health. Recently, many studies have shown that NO_2 levels in 2020 were lower than in previous years due to reduced anthropogenic emissions associated with reduced mobility during temporary lockdowns (e.g., Bauwens et al., 2020; Zander et al., 2020). Moreover, these NO_2 reductions in 2020 were associated with surface O_3 enhancement (Sicard et al., 2020b) and reduced O_3 levels in the free troposphere (Steinbrecht et al., 2021). Surface increases in O_3 in some cities were explained by a reduction of the NO titration effect (Sicard et al., 2020b).

Overall, data from various sources suggest a decline in worldwide mobility in 2020 (Nouvellet et al., 2021). Figure 1 shows the change in mobility (amount of people transiting public stations, derived from Google), compared to the pre-COVID

https://doi.org/10.5194/acp-2022-110
Preprint. Discussion started: 7 April 2022


Atmospheric Chemistry and Physics Discussions

period, for some large metropolitan areas around the world deeply affected by the pandemic (further details in Section 2.1.7). The larger reductions (with peaks over 90%) generally coincided with lockdowns, which occurred at slightly different times in different countries. Outside of lockdowns, mobility remained markedly decreased throughout 2020.

In Japan, the change in mobility was smaller and more gradual compared to other countries due to the lack of strict legal restrictions. However, on February 3, Japan began addressing the issue of the Diamond Princess cruise ship quarantine and on March 3, primary and secondary schools were closed and replaced with remote learning (Table 1). Then, an official state of emergency, when the most stringent restrictions were in effect, was declared from April 7 to May 25. Thereafter, the situation never returned to normal, as new periods of reduced mobility coincided with the second wave of coronavirus infections, which peaked in July–September, and the third wave starting in December.

Table 1. Milestones of the COVID-19 pandemic in Japan.

Date	**Milestone**
Jan. 15, 2020	First COVID-19 infection
Feb. 3, 2020	Diamond Princess cruise ship quarantine
Feb. 13, 2020	Japan confirms first COVID-19 death
Mar. 3. 2020	Schools closed
Mar. 11, 2020	WHO declares pandemic
Mar. 24, 2020	Tokyo Olympic Games postponed
Apr. 7 to May 25, 2020	State of emergency
Jul. 22, 2020	Government launches “Go To Travel” program
Jan. 7 to Mar. 7, 2021	State of emergency
Feb. 17, 2021	Japan begins COVID-19 vaccinations
Jul. 12 to Sep. 30, 2021	State of emergency
Jul. 23 to Aug. 8, 2021	Games of the XXXII Olympiad
Aug. 24 to Sep. 5, 2021	Tokyo 2020 Paralympic Games

Generally, the mean reduction in mobility was similar among all weekdays and slightly smaller during the weekend in most of the examined countries (Fig. 1b). In contrast to this worldwide trend, Japan showed the largest mobility drop during the weekend, with decreases about 10% larger than on weekdays. Although limited to the state of emergency period and the Tokyo area, this behavior has been observed from other data sources (e.g., Figure 2 in Sugawara et al., 2021) and appears to be a robust feature representing common Japanese habits modified by the spread of the pandemic.

https://doi.org/10.5194/acp-2022-110
Preprint. Discussion started: 7 April 2022


Atmospheric Chemistry and Physics Discussions

Due to this anomalous change in mobility, we suggest that the (relative) NO_2 weekend effect in 2020, primarily driven by traffic, may show peculiar characteristics in Japan. Potentially, this effect could be larger than usual, despite reduced NO_x emissions tending to reduce the anthropogenic weekly signature (Stavrakou et al., 2020). This unique situation provides the opportunity to examine the changes in the air quality that occurred in 2020 in Japan and compare them with previous years.

We focused our study on the Greater Tokyo Area (GTA), in the Kanto region, which is the most populous metropolitan area in the world and the largest area of flat land in Japan, extending inland from the Pacific coast (Fig. 2). Most of this large urban area is expected to be under VOC-limited conditions (Akimoto, 2017; Irie et al., 2021). In this study, we apply an integrated approach that exploits various independent datasets retrieved from multiple platforms, including observations of NO_2, O_3, and HCHO (as a proxy for non-methane VOC, NMVOC) from two sites equipped with Multi-Axis Differential Optical Absorption Spectroscopy (MAX-DOAS) systems located in urban and suburban areas. Further, anthropogenic light-absorbing aerosol data are presented. In contrast to most previous studies, which have focused on in situ and satellite-based data, observations representative of the boundary layer (< 1 km) provide our reference data to link surface and satellite column observations.

2 Datasets and methods

2.1 Datasets

2.1.1 MAX-DOAS

We used MAX-DOAS observations operated at Chiba University and Tsukuba sites, which are located in urban and semi-urban environments within the Kanto region (Fig. 2). The MAX-DOAS technique is based on the well-established DOAS technique (Platt and Stutz, 2008), which utilizes differential absorption structures of trace gases in ultraviolet (UV) and visible (VIS) wavelength regions to derive aerosol and trace gas information (Hönninger et al., 2004). Our MAX-DOAS system is equipped with a UV-VIS spectrometer located indoors, while an outdoor telescope unit collects scattered sunlight at reference and off-axis elevation angles. A set of scattered sunlight spectra was measured in a 15-min interval. High-resolution spectra were recorded from 310 to 515 nm (full width at half maximum, FWHM = 0.4 nm at 357 and 476 nm) and wavelength calibration was performed daily to account for potential spectrometer signal degradation. Retrieval was conducted based on DOAS and optimal estimation methods using the Japanese vertical profile retrieval algorithm version 2 (Irie et al., 2011, 2015) for the following purposes: DOAS fitting, retrieval of the aerosol profile and retrieval of trace gases. In this study, partial vertical columns of O_3, NO_2, and HCHO concentrations below 1 km were used. Notably, due to the contribution of upper troposphere/lower stratosphere (UT/LS) O_3 to differential slant column densities, only data collected at a solar zenith angle (SZA) below 50° can be used for O_3 retrieval (Irie et al. 2011, 2021). Therefore, the ozone dataset employed here was limited to the period of March–October. For cloud screening, measurements with retrieved aerosol optical depth (AOD) greater than 3 and relative humidity over water greater than 90% were excluded. The uncertainty in the retrieved profiles was further reduced by averaging the data from four collocated MAX-DOAS instruments pointing in four

https://doi.org/10.5194/acp-2022-110
Preprint. Discussion started: 7 April 2022


Atmospheric Chemistry and Physics Discussions

different directions at the Chiba site (see inset in Fig. 2). This procedure is expected to better account for the potential spatial heterogeneity of tropospheric gases. By contrast, observations from a single MAX-DOAS system were used for the Tsukuba site. The MAX-DOAS horizontal viewing distance depends on atmospheric conditions (i.e., aerosol load), and can be up to 24 km in the lowest 1-km vertical layer. Therefore, the MAX-DOAS partial column observations at Chiba are representative of the boundary layer across a region larger than a usual satellite pixel, but sampled at higher accuracy.

2.1.2 TROPOMI

The Tropospheric Monitoring Instrument (TROPOMI) onboard the European Union Copernicus Sentinel 5 Precursor (S5P) satellite has a Sun-synchronous orbit with a daily equator crossing time of approximately 13:30 local solar time and daily global coverage (van Geffen et al., 2019). The pixel size of TROPOMI was initially 3.5 × 7 km2 and was reduced to 3.5 × 5.6 km2 (August 2019), while the swath width is 2,600 km. The imaging spectrometer of this instrument measures radiation in the UV, VIS, near infrared, and shortwave infrared spectral regions (De Smedt et al. 2021; Veefkind et al., 2012). Operational level 2 (L2) products retrieved from TROPOMI observations include vertical columns of O_3, NO_2, HCHO, carbon monoxide (CO), sulfur dioxide (SO_2), and methane (CH_4). In the following analysis, we used the NO_2 and HCHO datasets recorded between January 2019 and December 2020, which were interpolated over a regular grid of 0.1 × 0.1°.

The TM5-MP-DOMINO NO_2 data used in this study are based on the DOMINO retrieval (van Geffen et al., 2019), previously used for Ozone Monitoring Instrument (OMI) data, and exploit the 405–465 nm spectral range to render tropospheric vertical column density with precision of 30–40%. The profile shape of the TM5-MP model is used for computation of the air mass factor (AMF) without accounting for aerosols. Screening of TROPOMI NO_2 data involved retaining data with a quality flag (QF) value higher than 0.5 and a cloud fraction (CF) lower than 0.2.

A retrieval algorithm developed for OMI QA4ECV products is used to retrieve TROPOMI L2 HCHO vertical column densities. HCHO slant column densities are retrieved in the 328.5–359 nm fitting window. The HCHO vertical columns are calculated from the retrieved slant column densities and AMF, which is based on TM5-MP. TROPOMI L2 cloud products provide cloud information for AMF calculations. A more explicit explanation of the TROPOMI HCHO retrievals and their validation is provided in the works of De Smedt et al. (2018, 2021). Data filtering was performed as detailed in the product read-me file (http://www.tropomi.eu/sites/default/files/files/publicSentinel-5P-Formaldehyde-Readme.pdf).

2.1.3 OMI

OMI is onboard the National Aeronautics and Space Administration (NASA) Aura satellite, which has a Sun-synchronous polar orbit. OMI passes the Equator around 13:40 LT (local time) and the size of its pixels is 13 km × 24 km at nadir.

We used OMI NO_2 Level-2 data (over Chiba University and Tsukuba sites) and the recently updated Level-3 daily global gridded (0.25 × 0.25°) OMNO2d data V4. The algorithm includes improved surface and cloud treatments (Lamsal et al., 2021). In the following analysis, we exploited observations recorded in 2005–2019, and screened out NO_2 data associated with a cloud fraction larger than 30%.

https://doi.org/10.5194/acp-2022-110
Preprint. Discussion started: 7 April 2022


Atmospheric Chemistry and Physics Discussions

2.1.4 Surface in situ and additional ground observations

In Japan, continuous monitoring of NO_x and other compounds through a capillary surface network is performed by the Atmospheric Environmental Regional Observation System (AEROS). Historical time-series data are accessible to the public via the geographic information system (GIS) of the National Institute for Environmental Studies (NIES) (http://www.nies.go.jp/igreen/index.html). As the most recent years are unavailable from the NIES catalog, we limited our analysis to NO_2 observations in 2015–2018. We used a total of 266 stations, including general atmosphere measurement stations and automobile exhaust gas measurement stations in Tokyo, Chiba and Ibaraki prefectures. The measurement principles of O_3, NO_x, and non-methane hydrocarbons are based on UV absorption, NO-O_3 chemiluminescence, and flame ionization detection, respectively.

In addition to the NIES dataset, we used observations of black carbon (BC) concentrations recorded by the continuous soot-monitoring system (COSMOS) (Kondo et al., 2009) deployed at Chiba University site in November 2019. Our analysis focused on observations recorded in 2020.

Finally, we combined optical property information retrieved by a sky radiometer with MAX-DOAS data to estimate light-absorbing aerosols within the boundary layer (Damiani et al., 2021), as described in Section 2.2.

2.1.5 CLASS model

Simulations with a box model accounting for boundary layer dynamics and chemistry were performed using the Chemistry Land-surface Atmosphere Soil Slab (CLASS) model (van Stratum et al., 2012; Vilà-Guerau de Arellano et al., 2015). In these simulations, we used fixed dynamic (i.e., the usual boundary layer height recorded by the collocated lidar instrument) and chemistry conditions (as in van Stratum et al., 2012), along with the concentrations of NO_2 and HCHO recorded by the MAX-DOAS system within the boundary layer (at altitudes lower than 1 km) as initial conditions. The model solves the diurnal evolution of dynamical and chemical species over time in a well-mixed convective planetary boundary layer (PBL) (Vilà-Guerau de Arellano et al., 2015). Since these variables are assumed to be constant with height, the model output approximates MAX-DOAS observations in the PBL. Chemistry is represented by an O_x-NO_x-VOC-HO_x photochemistry scheme based on 28 reactions that control O_3 formation. Although this simplified scheme omits other important organic species and aerosols, CLASS has been shown to reproduce the observed diurnal variability and mixing ratios of the main reactants present in polluted environments (Zara et al., 2021 and references therein).

2.1.6 Copernicus Atmosphere Monitoring Service (CAMS) global reanalysis

CAMS global reanalysis (EAC4) is the latest global reanalysis dataset of atmospheric composition produced by the European Centre for Medium-Range Weather Forecasts (ECMWF), including aerosols, chemical species and greenhouse gases (Innesset al., 2019). Atmospheric data are interpolated to 25 pressure levels (top level, 0.1 hPa) at a spatial resolution of 0.7 × 0.7°. Notably, both OMI (overpass at 1:30 pm) and GOME-2 (overpass at 10 am) NO_2 data are assimilated in

https://doi.org/10.5194/acp-2022-110
Preprint. Discussion started: 7 April 2022


Atmospheric Chemistry and Physics Discussions

CAMS, but anomalous emissions that occurred in 2020 are not included. Instead, CAMS uses MACCity anthropogenic emissions and the CO emissions upgrade described by Stein et al. (2014). Monthly mean VOC emissions were calculated using the MEGAN model.

2.1.7 Additional datasets

Ozonesonde observations were launched from the Tateno Aerological Observatory (Tsukuba, Japan) by the Japan Meteorological Agency (JMA), usually at 3 pm (i.e., around the anticipated time indicating maximum ozone). The KC ozonesonde used until November 2009 was replaced with an ECC ozonesonde in December 2009. In the following analysis, we used data recorded in the period of 2013–2020 for consistency with the MAX-DOAS time series.

MERRA-2 is NASA's latest reanalysis and includes online aerosol fields that interact with model radiation fields (Buchard et al., 2017; Randles et al., 2017). This product is based on coupling of the Goddard Earth Observing System, Version 5 Earth system model with the Goddard Chemistry Aerosol Radiation and Transport aerosol model. The resolution is 0.625 x 0.5 degree with 72 vertical layers from the surface to approximately 80 km. In the following analysis, we employed data for wind speed, temperature, and PBL height (PBLH).

Google Mobility data show changes to visits to various places worldwide (https://www.google.com/covid19/mobility/). Visits on each day are compared to baseline values for that day of the week. The baseline is the median value for the corresponding day of the week during the 5-week period of Jan 3–Feb 6, 2020. The following place categories are available: Grocery & pharmacy, Parks, Transit stations, Retail & recreation, Residential, and Workplaces. Here, we focused on changes in the Transit stations category (Fig. 1) in certain large metropolitan areas of the world deeply affected by the pandemic.

2.2 Methods

Except where otherwise noted, we focus on ground-based daily observations recorded between 9 am and 3 pm LT. Weekly changes in NO_2, HCHO, O_3, and light-absorbing aerosols are reported as differences with respect the average value on weekdays. As the strongest reduction of anthropogenic emissions occurs on Sunday in the investigated region, we refer to weekly changes as the difference between the Sunday value and the average of the weekdays. The holiday effect was estimated to be the difference between the average concentration of a given compound during the given holiday period and that in the two 10-day periods immediately before and after the holiday.

Light-absorbing aerosols within the boundary layer were estimated to be described in Damiani et al. (2021), combining sky radiometer and MAX-DOAS optical property data at UV wavelengths. Then, in the following analysis, we examine the fine-mode absorbing AOD within the partial column below 1 km (i.e., fAAOD [0–1 km]), which was computed by combining the columnar fine-mode fraction (FMF) and single scattering albedo (SSA) parameters retrieved from the sky radiometer with

https://doi.org/10.5194/acp-2022-110
Preprint. Discussion started: 7 April 2022


Atmospheric Chemistry and Physics Discussions

the mean partial column AOD estimated from MAX-DOAS measurements. As mineral dust can be strongly absorbing in the UV spectral range, we further removed days with Angstrom exponent (AE) < 1.

Composite differences between high and low wind speed in TROPOMI NO2 were computed based on MERRA-2 wind fields averaged around the overpass time (12–3 pm). The median wind speed of each pixel was assumed to be the threshold between the high and low wind composite values. We first regridded the MERRA-2 data to the resolution of TROPOMI; then, for each grid cell, we computed NO_2 as the difference between the composite values of days with high and low wind speed.

3 Results

3.1 Trends and seasonal changes

The spatial distribution of the TROPOMI NO_2 and HCHO column data in the Kanto region is shown in Fig. 3 for 2019 and 2020 on an annual basis (top panels) and during the state of emergency (bottom panels). The bulk of NO_2 is around Tokyo, which is the most densely populated area (Fig. 2), including along the main communication routes, and extends toward the south, where various large power plants and industrial activities are located (left column in Fig. 3). Overall, on an annual basis, column NO_2 over the GTA was reduced by about 10% in 2020 compared to 2019 (Fig. 3m), with larger absolute reductions around Haneda and Narita international airports, while smaller changes occurred in areas characterized by the presence of multiple power plants (South of Chiba). On the other hand, during the state of emergency, TROPOMI shows the largest NO_2 reduction (20–40%) in the southern Tokyo area while limited reductions (about 10%) occurred around Chiba and Tsukuba (Fig. 3o). Assuming that traffic currently contributes about 40% of Japanese domestic NO_x emissions (Kurokawa and Ohara, 2020), a drop in mobility by about 50% in April–May (Fig. 1) is consistent with the TROPOMI-based estimate of NO_2 changes related to COVID.

Aside from anthropogenic emissions, meteorological conditions contribute to determining the interannual variability of NO_2. Annual differences between 2020 and 2019 in major meteorological parameters such as wind speed, surface temperature and PBLH, which are expected to influence the NO_2 distribution, were quite limited (Fig. S1a–c). In contrast, during the state of emergency, the wind speed in 2020 was slightly higher than that of 2019 and potentially contributed to further reducing the NO_2 levels (Fig. S1d).

Although the uncertainties associated with column retrievals of HCHO are larger than for NO_2, the spatial distribution of the TROPOMI HCHO column was estimated (Panel (e–h) in Fig. 3). While NO_2 variability is dominated by anthropogenic activities, HCHO arises from both anthropogenic and natural sources. The main anthropogenic sources are vehicle exhaust emissions and industrial emissions, while the main natural sources are plants and biomass burning. Although the general increasing gradient from the ocean toward the continent resembles the pattern of NO_2, the HCHO distribution is not well defined and does not align the urbanized region. The somewhat higher HCHO concentration in 2020 (Fig. 3n), despite lower anthropogenic emissions, may be driven by small differences in temperature between the two years (Fig. S1b). However, the

https://doi.org/10.5194/acp-2022-110
Preprint. Discussion started: 7 April 2022


Atmospheric Chemistry and Physics Discussions

application of cloud screening caused a reduction in the available HCHO data, leading to somewhat different annual distributions of observed days in the two years. This confounding factor complicated the interpretation of HCHO changes. Then, despite the lower temperature that occurred during the state of emergency (Fig. S1e), TROPOMI did not show evident differences in the HCHO pattern between the two years (Fig. 3p).

The HCHO-to-NO_2 concentration ratio is an indicator of near-surface O_3 sensitivity (e.g., Martin et al. 2004). Although O_3 sensitivity derived from satellite column data can differ somewhat from that based on in situ observations (Schroeder et al. 2017), it nonetheless provides useful information and has been extensively studied in relation to COVID-19 (e.g., Ghahremanloo et al., 2021 among others). The HCHO/NO_2 ratios are shown in Fig. 3i–l. Overall, the ratio increased in 2020, indicating a shift toward more NO_x-limited conditions. This change is particularly evident for Tsukuba, where the ratio rose from 2.1 to 2.9, while limited variations occurred over Tokyo and Chiba. We can observe similar findings during the emergency period (Fig. 3k,l).

To further contextualize the changes that occurred in 2020, Fig. 4 shows monthly partial column NO_2, O_3, HCHO, as well as light-absorbing aerosols within the boundary layer (i.e., < 1 km) recorded at Chiba University. To better account for the spatial heterogeneity of tropospheric gases, the average values from four MAX-DOAS systems looking at different directions were employed (Section 2.1.1 and Fig. 2). As shown in a recent study (Irie et al., 2021), both NO_2 and HCHO were reduced and O_3 recovered slightly during the period of 2013–2019. Any potential COVID-related effects in 2020 were superimposed over these trends. Indeed, in 2020, NO_2 remained at its lowest recoded levels for almost the entire year, whereas HCHO was only occasionally lower in 2020 than 2019, particularly in the second half of the year, and no modulation of O_3 was evident. When analysis was limited to the period of the state of emergency (i.e., roughly April-May), all species considered here showed decreases in May compared with the same period of 2019 while some enhancements in April. This is coherent with an electricity demand reduction in May more significant than April for Chiba and the other Prefectures of the Kanto region (data from the Japanese Agency for Natural Resources and Energy available at https://www.enecho.meti.go.jp/statistics/electric_power/ep002/results_archive.html).

Overall, in agreement with the tropospheric column observations (Fig. 3o,p), slight changes occurred in the boundary layer around Chiba during the emergency period. In addition to the decrease in NO_2, similar month-to-month variabilities in HCHO and O_3 are apparent from the differences between 2020 and 2019.

As a further reference, we compared the observed changes with equivalent CAMS data, which assimilate satellite observations of tropospheric NO_2 (Section 2.1.6). CAMS data roughly reproduced the observed interannual and seasonal variabilities (Fig. 4). However, while the trends in NO_2 and O_3 were comparable to observations, CAMS did not reproduce the HCHO decrease; instead, an increasing trend was simulated. The month-to-month variability was very similar to that of observations. Nevertheless, the CAMS NO_2 difference between 2020 and 2019 was generally smaller than the observed difference (Fig. 4i). Although satellite NO_2 data are assimilated in CAMS, the impact of assimilation is expected to be limited for short-lived species such as NO_2 (Inness et al., 2019). Therefore, as CAMS simulations did not include the

https://doi.org/10.5194/acp-2022-110
Preprint. Discussion started: 7 April 2022


Atmospheric Chemistry and Physics Discussions

anomalous 2020 emissions, comparison of CAMS and MAX-DOAS datasets supports the possibility that the emissions reduction in 2020 was responsible for the observed stronger NO_2 decrease. On the other hand, CAMS satisfactorily reproduced the month-to-month variabilities of both O_3 and HCHO.

Finally, we considered the changes in light-absorbing aerosol in both the boundary layer and the total column. Although this dataset is characterized by high uncertainty (Damiani et al., 2021), the values in 2020 were clearly the lowest on record. The largest relative changes (not shown) occurred before the state of emergency (i.e., in January and February), while the largest absolute change occurred in fall; nonetheless, some reduction was apparent in May. In this huge urbanized region, light-absorbing aerosols tend to be produced mainly by local pollution. However, transboundary transport has been shown to further modulate the light-absorbing aerosol dataset (Damiani et al., 2021), complicating the attribution of effects to the pandemic.

3.2 Weekend, holiday, and wind effects from various platforms

Previous studies (e.g., Beirle et al., 2003) have reported that apparent signatures of anthropogenic activity reflect a weekly cycle of NO_2 over most major cities in the northern hemisphere. To contextualize the weekly changes occurring in the GTA, we analyzed global OMI NO_2 data for the period of 2005–2020. Figure 5a shows the global ranking of the resulting relative changes on Sunday over cities with population larger than 0.5 million inhabitants (we implicitly excluded cities where the rest day is on Friday). For the sake of clarity, we report only those cities with changes more prominent than 30%, although the majority of locations showed negative values (except in China; Stavrakou et al., 2020). Japanese cities dominate the histogram; worldwide, the extent of changes over the GTA is exceeded only by Los Angeles and São Paulo. The OMI-based map of such changes (Fig. 5b) shows a well-defined pattern over Japan, with consistent values negative across the country, which were lower than –40% over most of the GTA and industrialized regions in southern Japan (i.e., Nagoya, Osaka).

Power plants and other industrial facilities are the dominant stationary emissions sources, and are generally consistent, with little effect of weekly modulation. Satellite NO_2 data can be used to investigate both stationary (Beirle et al., 2019) and mobility-related emissions sources (Ialongo et al., 2020). Using satellite NO_2 and wind field data, emissions related to large and isolated stationary sources can be assessed (Beirle et al., 2019). Nevertheless, when multiple stationary sources are located within an urbanized region, as in our study area, evaluating the impacts of the various sources becomes challenging. As shown in Fig. 5c, we exploited the high resolution of TROPOMI data to compare NO_2 changes associated with the weekly cycle (i.e., Sunday minus weekdays) to NO_2 changes associated with wind speed in 2019–2020. Moreover, to better highlight the spatial patterns of these changes, we focused on the extended summer period from April to September, when the NO_2 lifetime is shorter and NO_2 tracks emissions sources better. Both contour lines suggest larger reductions over Tokyo than other areas, with patterns mostly matching the spatial distribution of population density. The weekly related NO_2 generally extends north to Tsukuba and east to Chiba with a roughly homogeneous spatial gradient, while the gradient sharpens south of Chiba.

https://doi.org/10.5194/acp-2022-110
Preprint. Discussion started: 7 April 2022


Atmospheric Chemistry and Physics Discussions

During days characterized by stagnant wind conditions, NO_2 levels tend to accumulate around stationary sources, while rapid transport occurs with stronger winds. In addition to covering areas with high population density, high negative wind-related changes are apparent around the main power plants on both sides of Tokyo Bay. Moreover, detailed distributions around stationary sources have been revealed (e.g., changes around Narita international airport and the isolated Kashima power plant on the east coast of Chiba Peninsula). Overall, the distribution of wind-related changes is more southerly than the bulk of weekly changes. Moreover, this gradient becomes positive in the north, highlighting the region downwind of the Tokyo area, including Tsukuba. Overall, wind-related NO_2 changes closely resemble the pattern shown in the Japanese Emission Inventory.

The map in Fig. 5d shows the NO_2 decrease occurring during the end-of-year holiday, when most anthropogenic emissions are reduced. To quantify this holiday effect, the average NO_2 value of the 10 days before and after the holiday (defined here as the period from 25 December to 4 January) was subtracted from the holiday mean. Figure 5d shows similar patterns to Fig. 5b, although the longer NOx lifetime in winter causes the changes to be less confined to urbanized regions. TROPOMI NO_2 decreased by about –43 and –49% in Chiba and Tsukuba, respectively (Fig. S2). The holiday effect is apparent in almost all cities with intense weekly cycles (Fig. 5a) and will be used as a further reference.

Multi-year MAX-DOAS observations of partial column NO_2 recorded at Chiba University also showed a decrease around the end of the year (Fig. S2). It was about –44%, while smaller changes occurred in HCHO (about –15%). Slightly larger reductions were observed at Tsukuba site (–55% and 29%, for NO_2 and HCHO, respectively).

Focusing on the holiday period provides insights into the response of O_3 to these significant changes. As only data at SZA lower than 50° can be used to retrieve O_3 with the DOAS method (Irie et al. 2011; see Sect. 2), we focused on ozonesonde profiles recorded at the Tateno Observatory, located about 50 km from Chiba. In this manner, we assessed the vertical distribution of O_3 changes within and slightly above the PBL. These data were used to better interpret the changes in partial column O_3 estimated by the MAX-DOAS systems. In the lower troposphere, the average O_3 profile concentration averaged across business days was smaller than the O_3 concentration recorded during the end-of-year holiday (Fig. 5e). The difference was greatest in the lowest layers (about –18%) and remained nearly constant up to 0.5 km; then, it became smaller and disappeared above 1 km. The reduced NO titration effect occurring under VOC-limited conditions is likely the main driver of this peculiar pattern of increased O_3 levels in the lowest layers during the holiday period.

We simulated the periods of 2019 and 2020 with the CLASS model using the appropriate mean NO_2 and HCHO observations and lidar-based PBLH recorded at Chiba as initial conditions. The results of the simulations (vertical lines in Fig. 5e) confirmed the holiday-associated positive O_3 enhancement, with a relative difference of 22% at 15:00 LT, which was also the time of the sonde launch corresponding to the diurnal ozone peak. Previous studies have reported comparable O_3 enhancement effects on the weekend, particularly in winter (Sadanaga et al., 2012; Sicard et al., 2020a). Using the same approach, we evaluated the changes occurring around mid-August, which is a period of reduced mobility. Such changes are interesting in terms of the O_3 formation regime, but significant variability prevented clear identification of trends (Fig. S2).

https://doi.org/10.5194/acp-2022-110
Preprint. Discussion started: 7 April 2022


Atmospheric Chemistry and Physics Discussions

Figure 6 further characterizes the NO_2 weekend effect and contextualizes the holiday effect through comparison of ground-based partial column (< 1 km), satellite-based tropospheric column, and surface in situ observations. In Chiba, relocation of all four instruments occurred in 2014 (i.e., the pointing direction of some sensors was changed slightly; Irie et al., 2021); therefore, in the following analysis, we excluded observations recorded in 2013 and 2014. Panel (a) shows the geographic distribution of NO_2 weekly changes on Sunday for OMI, with MAX-DOAS and in situ observations plotted together. We focused on 2015–2018, when all three datasets were available. The spatial distribution of OMI NO_2 is as shown in Fig. 5b. The largest negative changes occurred over Tokyo, which reached –45%, and changes became smaller toward Chiba and Tsukuba. Notably, the magnitude of these changes is larger around Tsukuba (–35%) than around Chiba (–30%), although Tsukuba is a suburban site, while the urban area of Chiba hosts a larger population (Fig. 2) and industrial activities. In situ observations match the satellite-based spatial distribution, although with a somewhat smaller magnitude (by about 5%).

MAX-DOAS partial column data reproduced the spatial distribution of the previous datasets (inset in Fig. 6a), showing a magnitude of change slightly closer to that of OMI (i.e., total column) than the surface network. Both in situ and MAX-DOAS observations were averaged over 9 am–3 pm, while OMI observations were generally recorded around 1:30 pm. The small incongruence among measurements is likely due to the different sampling periods (i.e., while in situ observations include data recorded under all meteorological conditions, satellite and MAX-DOAS data were limited to clear-sky days).

We also compared the climatology of the weekly cycle from various platforms according to data availability (excluding 2020). For comparison with the other datasets, we used the mean value from the in situ stations within Chiba (Fig. 6b) and Ibaraki (Fig. 6c) prefectures, respectively. Despite the different periods analyzed, the weekly cycles were very similar for all three platforms. The magnitude of change is largest on Sunday; at Chiba, OMI changes are approximately 10% larger than both ground observation types. By contrast, at Tsukuba, in situ data are lower than OMI and MAX-DOAS by 10–15% (but due to the scarcity of in situ stations around Tsukuba, the average value of stations inside Ibaraki prefecture is likely not representative of the area around Tsukuba). In addition to Sunday, indications of reduced NO_2 are apparent on Friday and Saturday at both sites. As a further reference, we included the NO_2 weekly cycle of Tokyo Prefecture. The data confirmed that weekly cycles are similar in the three prefectures, with values for Tokyo on Sundays being about 5–10% larger than in other prefectures.

Figure 6d and 6e show changes in OMI NO_2 on Sunday averaged over the periods of 2005–2007, 2015–2019, and 2005–2019 at Chiba and Tsukuba, respectively. The OMI NO_2 column over the investigated region decreased by about 50% over 2005–2019 (see Fig. S3 for Chiba). Therefore, in accordance with a previous study (Stavrakou et al., 2020), the weekly cycle showed a reduced amplitude in recent years. During this latest period, in situ, satellite, and MAX-DOAS observations at Chiba coincided, while these data sources showed a spread of about 15% at Tsukuba. This larger variability at Tsukuba is likely due to its lower NO_2 levels and suburban location downwind of the Tokyo area (Fig. 5c).

As a further reference, Fig. 6d,e also show the end-of-year holiday reductions. Overall, when considering the full 2005–2019 period, OMI holiday changes were larger than OMI Sunday changes by about 8% for both Chiba and Tsukuba. However, in recent years, NO_2 values were much larger on holidays than on Sundays.

https://doi.org/10.5194/acp-2022-110
Preprint. Discussion started: 7 April 2022


Atmospheric Chemistry and Physics Discussions

For Chiba, the distinct Sunday changes recorded by each of the four MAX-DOAS instruments were also investigated. The instruments showed a spread of less than 10% with limited interannual variability. The amplitude of the NO_2 weekend effect differed among instruments, with smaller effects for the instruments pointing south and east than for those pointing north and west. This difference was likely due to the presence of power plants and industrial activities within a few tens of km south of the sampling site, providing an additional and more constant emissions source that reduces the difference between rest and business days. Indeed, absolute NO_2 amounts were generally higher for the MAX-DOAS facing south, followed by the east-, west-, and finally north-facing instruments (inset in Fig. S3).

Moreover, changes in MAX-DOAS NO_2 were much more prominent in 2020 than in previous years. Notably, 2020 was equally anomalous for all instruments, with decreases around 15–20%. Therefore, the observed decrease was not a local phenomenon. Generally, MAX-DOAS changes at Tsukuba are more significant than the data recorded at Chiba. Nevertheless, at Tsukuba, changes in 2020 were within the usual level of interannual variability. Therefore, the anomalous weekly cycle in 2020 affected the urban region of Chiba but not suburban area.

3.3 Weekly cycles

3.3.1 Weekly cycle of partial column NO_2, HCHO, O_3 and light-absorbing aerosols

Figure 7 shows the interannual weekly changes in MAX-DOAS partial columns of NO_2, HCHO, O_3, and HCHO/NO_2 at Chiba and Tsukuba sites. Further changes in fAAOD [0–1 km] were reported for Chiba only. As we used observations averaged over four independent MAX-DOAS systems at Chiba, the data are more statistically robust and representative of a larger area than observations from Tsukuba (sampled with only one instrument). Therefore, most of the following discussion on interannual changes is focused on Chiba.

As noted above, at Chiba, while the NO_2 change on Sunday was approximately –30% for 2015–2019, it reached about –45% in 2020. This difference was much larger than 2 × sigma (Fig. S4). On the other hand, except in 2020, interannual variability was much smaller on Sunday than on other days. By contrast, at Tsukuba, Sunday changes in 2020 were comparable to those in previous years.

Usually, the weekend effect was absent in HCHO data from both Chiba and Tsukuba. Nevertheless, at Chiba, negative HCHO changes on Sunday 2020 were unprecedentedly large (around –30%). This negative anomaly is larger than the largest deviation on any other day in previous years, and can be attributed to abnormally low anthropogenic NMVOC on the Sundays of 2020 (Sun et al., 2021; Ghahremanloo et al., 2021). By contrast, HCHO showed no unusual trends at Tsukuba in 2020, and this difference is likely due to differences in local conditions (i.e., Tsukuba is located in a suburban area, where a greater amount of biogenic VOC emissions contribute to HCHO concentrations) and higher variability associated with the usage of only one instrument.

A weekly cycle in the HCHO/NO_2 ratio is evident for Tsukuba, with its peak on Sunday (approximately double the weekday average). On the other hand, for Chiba, the slightly higher ratio on Sunday was similar to the value on weekdays (0.55 vs.

https://doi.org/10.5194/acp-2022-110
Preprint. Discussion started: 7 April 2022


Atmospheric Chemistry and Physics Discussions

0.4). Notably, on almost all days of 2020, the HCHO/NO_2 ratio at Tsukuba was higher than in previous years, while no difference was recorded at Chiba.

Despite this large variation in the main precursors, corresponding modulations in the O_3 partial column were not recorded on Sundays of 2020 or previous years. Although the amplitude of the weekend effect in ozone is likely to have been reduced in recent years (Sicard et al., 2020a), its absence in our data contrasts with previous results showing a discernible weekend effect in surface ozone at Tokyo (Sadanaga et al., 2012). Ozone in the free troposphere presents a greatly smoothed diurnal cycle, if any, compared to surface ozone and this diurnal cycle is generally strongest below 950 hPa (Petetin et al., 2016). Moreover, Fig. 5e suggests that any potential change in O_3 in response to NO_2 changes should have occurred mostly below 0.5 km. Therefore, due to the increase in O_3 concentration with the altitude and the limited number of O_3 observations compared to other compounds, any potential weekly cycle would be difficult to observe in our MAX-DOAS O_3 partial column dataset.

We further evaluated potential ozone differences between Sundays and weekdays of 2015–2020 using the box model (not shown). As in the previous simulations, we used MAX-DOAS observations of NO_2 and HCHO and lidar-based PBLH as initial conditions and focused on the period most strongly affected by the pandemic (i.e., April–September). The simulated ozone differences between Sundays and weekdays were slightly negative (i.e., Sunday O_3 < weekday O_3) and ranged from –4% in 2018 to –8% in 2020.

As shown in the bottom panel, we examined the weekly cycle of fAAOD partial column data at Chiba. Although such data are characterized by high interannual variability, similar to the results presented above, 2020 data were anomalous, characterized by negative changes of about 50% on Sunday and no variation on Saturday. Notably, consistent with the results for NO_2 (Fig. 6d), changes in fAAOD on Sundays in 2020 are comparable with the effect usually observed during the end-of-year holiday. Although the weekly cycle is hardly discernible in the other years, the weekly cycle in 2020 is coherent with that of collocated observations of surface BC mass concentration, which show reductions larger than 40% on Sunday and no change on Saturday.

We further excluded the influence of meteorology on the observed interannual variation by examining data on wind speed, wind direction, and temperature recorded at Chiba on days with available MAX-DOAS observations (Fig S5). Overall, the results showed that wind did not drive the weekly changes in tropospheric gases. As increasing temperature enhances biogenic emissions and boosts oxidation processes, temperature is usually positively correlated with HCHO. We verified the absence of apparent weekly variation in temperature. Moreover, due to the large amount of data recorded at Chiba site, we could confirm that weekly changes around the satellite overpass time were representative of the daily NO_2. No apparent difference between MAX-DOAS daily NO_2 for 9:00–15:00 and for 12:00–15:00 was observed (the same result was obtained for HCHO and O_3).

https://doi.org/10.5194/acp-2022-110
Preprint. Discussion started: 7 April 2022


Atmospheric Chemistry and Physics Discussions

3.3.2 Weekly cycle of TROPOMI NO_2 tropospheric columns

Next, we examined the pattern of weekly changes in TROPOMI NO_2, looking for differences in the spatial distribution and magnitude of Sunday changes between 2019 and 2020 (Fig. 8). Overall, changes were larger in 2020 than in 2019, reaching –50% over central Tokyo. Moreover, during the extended summer period (April to September), when the largest influence of COVID is expected, differences between 2020 and 2019 were even more apparent. In addition to the magnitude of the differences, the area characterized by higher NO_2 concentrations was greatly reduced in 2020 compared to 2019. This reduction averaged about –27% for weekdays and reached –67% for Sundays (Fig. S6).

Within the areas sampled by the MAX-DOAS systems, TROPOMI showed no clear differences between 2019 and 2020 in either Chiba or Tsukuba. For Chiba, this contrasts with ground observations. Different time windows, over which the daily means were computed (i.e., between 9 am and 3 pm for MAX-DOAS and around 1.30 pm for TROPOMI), and cloud screening procedures resulted in a larger amount of MAX-DOAS data than satellite data and likely contributed to these differences. However, despite being based on one year of observations, both TROPOMI maps could correctly reproduce the spatial pattern of changes estimated from ground-based observations around Chiba, i.e., the north-south gradient driven by the presence of power plants. This similarity provides confidence in identifying the interannual variability of the spatial distribution of the NO_2 weekly cycle based on TROPOMI data.

4. Discussion and conclusions

This study investigated the interannual, seasonal, weekly variabilities and spatial distributions in NO_2, HCHO, O_3, and light-absorbing aerosols measured with multiple platforms within the Greater Tokyo Area, which is the most populous metropolitan area in the world. We mainly examined the period of 2013–2020, focusing on 2020, when an effect from COVID-19 is expected. The main results can be summarized as follows:

- In 2020, levels of NO_2 and light-absorbing aerosols were the lowest on record, but the potential COVID-19 impact was superimposed on a decreasing trend.
- At Chiba, MAX-DOAS observations within the PBL showed that annual NO_2 reductions in 2020 were about 10% relative to 2019 with limited changes during the period of the state of emergency. No deviations in O_3 and HCHO were apparent.
- TROPOMI column-based observations confirmed the observed reduction in NO_2 and the absence of relevant changes in HCHO. During the state of emergency, NO_2 reductions exceeded 40% in the southern Tokyo area but were about 10% over Chiba and Tsukuba. Moreover, both satellite and MAX-DOAS observations showed enhancement of the HCHO/NO_2 ratio, which was strongest in the suburban region.
- OMI observations demonstrated that the weekly and holiday effects in NO_2 within the GTA are among the largest in the world. NO_2 reductions on rest days are not limited to the GTA but extend uniformly over most of Japan.

https://doi.org/10.5194/acp-2022-110
Preprint. Discussion started: 7 April 2022

• Surface in situ, MAX-DOAS partial column and satellite-based tropospheric column observations showed a coherent NO_2 weekly cycle, with the largest reductions on Sunday. Ground observations aligned with the spatial distribution of the satellite changes, even within the relatively limited area sampled by the MAX-DOAS systems.

• In 2020, ground and satellite observations showed an anomalous weekly cycle in NO_2 in urban areas, with larger reductions on Sunday than in previous years. Similar large changes in light-absorbing aerosols were identified. Such changes are comparable to the reductions observed during the end-of-year holiday period.

• At Chiba, large NO_2 reductions on Sunday were coupled with simultaneous reduction of HCHO, whereas no significant changes in O_3 were observed.

• In Japan, the reduction in mobility in 2020 was more extensive on the weekend than on business days, in accordance with the larger NO_2 weekly change in 2020 found in the urban areas. By contrast, other countries generally showed the opposite behavior. This highlights modification of habits by the Japanese populace that resulted in unique air quality effects, suggesting widespread adoption of recommendations aimed at limiting the spread of the pandemic in Japan despite the lack of strict legal restrictions.

Data availability. All datasets used in the present study are publicly available below:

https://www.temis.nl/

https://disc.gsfc.nasa.gov/

https://woudc.org/

https://www.google.com/covid19/mobility/

http://atmos3.cr.chiba-u.jp/skynet/

http://atmos3.cr.chiba-u.jp/a-sky/

https://www.ecmwf.int/en/forecasts/dataset/cams-global-reanalysis

http://www.nies.go.jp/igreen/index.html

Author contribution. Conceptualization, A.D.; Methodology A.D. and R.C.C.; Measurements and data curation, H.I.; Analysis, A.D., D.B., S.H.H., and S.K.; Funding acquisition: H.I.; Writing—review and editing, A.D., H.I., D.B., R.R.C.; all authors have read and agreed to the published version of the manuscript.

Competing interests. The authors declare that they have no conflict of Interest.

Acknowledgements. This research was supported by the Environment Research and Technology Development Fund (JPMEERF20192001 and JPMEERF20215005) of the Environmental Restoration and Conservation Agency of Japan, JSPS KAKENHI (grant numbers JP19H04235, JP20H04320, and JP21K12227), and the JAXA 2nd research announcement on the

Earth Observations (grant number 19RT000351). The authors would like to thank the OMI and TROPOMI Science Teams for the data products, CAMS and MERRA-2 for the corresponding reanalysis data products, and JMA, AEROS & NIES staff.

505

References

Akimoto, H., 2017. Overview of policy actions and observational data for PM2.5 and O3 in Japan: a study of urban air quality improvement in Asia. JICA-RI Working Paper 137

Bauwens, M., Compernolle, S., Stavrakou, T., Müller, J.-F., van Gent, J., Eskes, H., et al., 2020. Impact of coronavirus
510 outbreak on NO2 pollution assessed using TROPOMI and OMI observations. Geophysical Research Letters 47, e2020GL087978. https://doi.org/10.1029/2020GL087978

Beirle, S., Borger, C., Dörner, S., Li, A., Hu, Z., Liu, F., Wang, Y. and Wagner, T., 2019 Pinpointing nitrogen oxide emissions from space, Sci. Adv. 5(11). doi:10.1126/sciadv.aax9800.

Beirle, S., Platt, U., Wenig, M. & Wagner, T., 2003. Weekly cycle of NO2 by GOME measurements: a signature of
515 anthropogenic sources. Atmos. Chem. Phys. 3, 2225–2232.

Cleveland, W.S., Graedel, T.E., Kleiner, B. and Warner, J.L., 1974. Sunday and workday variations in photochemical air pollutants in New Jersey and New York. Science 186, 1037–1038. doi:10.1080/10473289.2003.10466222

Damiani, A., Irie, H., Yamaguchi, K., Hoque, H. M. S., Nakayama, T., Matsumi, Y., Kondo, Y., and Da Silva, A., 2021. Variabilities in PM2.5 and black carbon surface concentrations reproduced by aerosol optical properties estimated by in-situ
520 data, ground based remote sensing and modeling. Remote Sens. 13, 3163. https://doi.org/10.3390/rs13163163.

De Smedt, I., Pinardi, G., Vigouroux, C., Compernolle, S., Bais, A., Benavent, N., Boersma, F., Chan, K.-L., Donner, S., Eichmann, K.-U., Hedelt, P., Hendrick, F., Irie, H., Kumar, V., Lambert, J.-C., Langerock, B., Lerot, C., Liu, C., Loyola, D., Piters, A., Richter, A., Rivera Cárdenas, C., Romahn, F., Ryan, R. G., Sinha, V., Theys, N., Vlietinck, J., Wagner, T., Wang, T., Yu, H., and Van Roozendael, M., 2021. Comparative assessment of TROPOMI and OMI formaldehyde observations and
525 validation against MAX-DOAS network column measurements. Atmos. Chem. Phys. 21, 12561–12593. https://doi.org/10.5194/acp-21-12561-2021.

De Smedt, I., Theys, N., Yu, H., Danckaert, T., Lerot, C., Compernolle, S., Van Roozendael, M., Richter, A., Hilboll, A., Peters, E., Pedergnana, M., Loyola, D., Beirle, S., Wagner, T., Eskes, H., van Geffen, J., Boersma, K. F., and Veefkind, P., 2018. Algorithm theoretical baseline for formaldehyde retrievals from S5P TROPOMI and from the QA4ECV project,
530 Atmos. Meas. Tech. 11, 23952426. https://doi.org/10.5194/amt-11-2395-2018.

Geddes, J.A., Martin, R.V., Boys, B.L., van Donkelaar, A., 2016. Long-term trends worldwide in ambient NO2 concentrations inferred from satellite observations. Environ Health Perspect 124, 281–289. http://dx.doi.org/10.1289/ehp.1409567

Georgoulias, A. K., van der A, R. J., Stammes, P., Boersma, K. F., and Eskes, H. J., 2019. Trends and trend reversal detection in 2 decades of tropospheric NO2 satellite observations. Atmos. Chem. Phys. 19, 6269–6294. https://doi.org/10.5194/acp-19-6269-2019.

Ghahremanloo, M., Lops, Y., Choi, Y., Mousavinezhad, S., 2021. Impact of the COVID-19 outbreak on air pollution levels in East Asia. Science of The Total Environment, 754. 142226. ISSN 0048-9697. https://doi.org/10.1016/j.scitotenv.2020.142226

Hamra, G. B., Laden, F., Cohen, A. J., Raaschou-Nielsen, O., Brauer, M., & Loomis, D., 2015. Lung Cancer and Exposure to Nitrogen Dioxide and Traffic: A Systematic Review and Meta-Analysis. Environmental health perspectives 123(11), 1107–1112. https://doi.org/10.1289/ehp.1408882

Hönninger, G.; Von Friedeburg, C.; Platt, U., 2004. Multi axis differential optical absorption spectroscopy (MAX-DOAS). Atmos. Chem. Phys. 4, 231–254.

Ialongo, I., Virta, H., Eskes, H., Hovila, J., and Douros, J., 2020. Comparison of TROPOMI/Sentinel-5 Precursor NO2 observations with ground-based measurements in Helsinki. Atmos. Meas. Tech. 13, 205–218. https://doi.org/10.5194/amt-13-205-2020.

Inness, A., Ades, M., Agustí-Panareda, A., Barré, J., Benedictow, A., Blechschmidt, A.-M., Dominguez, J. J., Engelen, R., Eskes, H., Flemming, J., Huijnen, V., Jones, L., Kipling, Z., Massart, S., Parrington, M., Peuch, V.-H., Razinger, M., Remy, S., Schulz, M., and Suttie, M., 2019. The CAMS reanalysis of atmospheric composition. Atmos. Chem. Phys. 19, 3515–3556. https://doi.org/10.5194/acp-19-3515-2019.

Irie, H., Takashima, H., Kanaya Y., Boersma, K.F., Gast, L., Wittrock, F., Brunner, D., Zhou, Y., Van Roozendael, M., 2011. Eight-component retrievals from ground-based MAX-DOAS observations. Atmos. Meas. Tech. 4(6), 1027–1044. https://doi.org/10.5194/amt-4-1027-2011

Irie, H., Yonekawa, D., Damiani, A., et al., 2021. Continuous multi-component MAX-DOAS observations for the planetary boundary layer ozone variation analysis at Chiba and Tsukuba, Japan, from 2013 to 2019. Prog Earth Planet Sci 8, 31.

Irie, H., Nakayama, T., Shimizu, A., Yamazaki, A., Nagai, T., Uchiyama, A., Zaizen, Y., Kagamitani, S., Matsumi, Y., 2015. Evaluation of MAX-DOAS aerosol retrievals by coincident observations using CRDS, lidar, and sky radiometer in Tsukuba, Japan. Atmos. Meas. Tech. 8, 2775–2788.

Kondo, Y., Sahu, L., Kuwata, M., Miyazaki, Y., Takegawa, N., Moteki, N., Imaru, J., Han, S., Nakayama, T., Kim, O.N.T., et al., 2009. Stabilization of the mass absorption cross section of black carbon for filter-based absorption photometry by the use of a heated inlet. Aerosol Sci. Technol. 43, 741–756.

Kurokawa, J. and Ohara, T., 2020. Long-term historical trends in air pollutant emissions in Asia: Regional Emission inventory in ASia (REAS) version 3. Atmos. Chem. Phys. 20, 12761–12793. https://doi.org/10.5194/acp-20-12761-2020, 2020

Lamsal, L. N., Krotkov, N. A., Vasilkov, A., Marchenko, S., Qin, W., Yang, E.-S., Fasnacht, Z., Joiner, J., Choi, S., Haffner, D., Swartz, W. H., Fisher, B., and Bucsela, E., 2021. Ozone Monitoring Instrument (OMI) Aura nitrogen dioxide standard

product version 4.0 with improved surface and cloud treatments. Atmos. Meas. Tech. 14, 455–479. https://doi.org/10.5194/amt-14-455-2021.

Lee, H.-J., Chang, L.-S., Jaffe, D.A., Bak, J., Liu, X., Abad, G.G., Jo, H.-Y., Jo, Y.-J., Lee, J.-B., Kim, C.-H., 2021. Ozone Continues to Increase in East Asia Despite Decreasing NO2: Causes and Abatements. Remote Sensing. 13(11):2177. https://doi.org/10.3390/rs13112177

Li K, Jacob DJ, Liao H, Shen L, Zhang Q, Bates KH. Anthropogenic drivers of 2013–2017 trends in summer surface ozone in China. Proc Natl Acad Sci USA. (2019) 116:422–7. doi: 10.1073/pnas.1812168116

Murphy, J. G., Day, D. A., Cleary, P. A., Wooldridge, P. J., Millet, D. B., Goldstein, A. H., and Cohen, R. C., 2007. The weekend effect within and downwind of Sacramento – Part 1: Observations of ozone, nitrogen oxides, and VOC reactivity. Atmos. Chem. Phys. 7, 5327–5339. https://doi.org/10.5194/acp-7-5327-2007.

Nouvellet, P., Bhatia, S., Cori, A. et al., 2021. Reduction in mobility and COVID-19 transmission. Nat. Commun. 12, 1090. https://doi.org/10.1038/s41467-021-21358-2

Petetin, H., Thouret, V., Athier, G., Blot, R., Boulanger, D., Cousin, J.-M., Gaudel, A., Nédélec, P., Cooper, O., 2016. Diurnal cycle of ozone throughout the troposphere over Frankfurt as measured by MOZAIC-IAGOS commercial aircraft. Elem. Sci. Anth. 4, 129.

Platt, U., and Stutz, J., 2008. Differential optical absorption spectroscopy, principles and applications. Springer, XV, 597 p. 272 illus., 29 in color, Physics of Earth and Space Environments, ISBN 978-3-540-21193-8

Russell, A. R., Valin, L. C., and Cohen, R. C., 2012. Trends in OMI NO2 observations over the United States: effects of emission control technology and the economic recession. Atmos. Chem. Phys. 12, 12197–12209. https://doi.org/10.5194/acp-12-12197-2012.

Sadanaga, Y., Sengen, M., Takenaka, N. and Bandow, H., 2012. Analyses of the Ozone Weekend Effect in Tokyo, Japan: Regime of Oxidant (O3 + NO2) Production. Aerosol Air Qual. Res. 12: 161-168. https://doi.org/10.4209/aaqr.2011.07.0102

Sicard P., et al., 2020a. Ozone weekend effect in cities: Deep insights for urban air pollution control, Environmental Research 191, 110193. https://doi.org/10.1016/j.envres.2020.110193.

Sicard P., et al., 2020b. Amplified ozone pollution in cities during the COVID-19 lockdown, Science of The Total Environment 735, 139542

Stavrakou, T., Müller, J.-f., Bauwens, M., Boersma K. f. & van Geffen, J., 2020. Satellite evidence for changes in the no2 weekly cycle over large cities. Scientific Reports 10:10066, https://doi.org/10.1038/s41598-020-66891-0.

Steinbrecht, W., Kubistin, D., Plass-Dülmer, C., Davies, J., Tarasick, D. W., Gathen, P., et al., 2021. COVID-19 crisis reduces free tropospheric ozone across the Northern Hemisphere. Geophysical Research Letters 48, e2020GL091987. https://doi.org/10.1029/2020GL091987

Sugawara, H., Ishidoya, S., Terao, Y., Takane, Y., Kikegawa, Y., & Nakajima, K., 2021. Anthropogenic CO2 emissions changes in an urban area of Tokyo, Japan, due to the COVID-19 pandemic: A case study during the state of emergency in April–May 2020. Geophysical Research Letters 48, e2021GL092600. https://doi. org/10.1029/2021GL092600

Sun, W., Zhu, L., De Smedt, I., Bai, B., Pu, D., Chen, Y., et al., 2021. Global significant changes in formaldehyde (HCHO) columns observed from space at the early stage of the COVID-19 pandemic. Geophysical Research Letters 48, e2020GL091265. https://doi.org/10.1029/2020GL091265

Tan, P.-H., Chou, C., Liang, J.-Y., Chou, C. C.-K., Shiu, C.-J., 2009. Air pollution "holiday effect" resulting from the Chinese New Year. Atmospheric Environment 43, 2114-2124. ISSN 1352-2310. https://doi.org/10.1016/j.atmosenv.2009.01.037.

van Geffen, J.H.G.M., et al., 2019. TROPOMI ATBD of the total and tropospheric NO2 data products. Report S5P-KNMI-L2-0005-RP, KNMI, De Bilt, The Netherlands.

van Stratum, B. J. H., Vilà-Guerau de Arellano, J., Ouwersloot, H. G., van den Dries, K., van Laar, T. W., Martinez, M., Lelieveld, J., Diesch, J.-M., Drewnick, F., Fischer, H., Hosaynali Beygi, Z., Harder, H., Regelin, E., Sinha, V., Adame, J. A., Sörgel, M., Sander, R., Bozem, H., Song, W., Williams, J., and Yassaa, N., 2012. Case study of the diurnal variability of chemically active species with respect to boundary layer dynamics during DOMINO. Atmos. Chem. Phys. 12, 5329–5341. https://doi.org/10.5194/acp-12-5329-2012, 2012.

Veefkind, J. P., Aben, I., McMullan, K., Förster, H., de Vries, J., Otter, G., Claas, J., Eskes, H. J., de Haan, J. F., Kleipool, Q., van Weele, M., Hasekamp, O., Hoogeveen, R., Landgraf, J., Snel, R., Tol, P., Ingmann, P., Voors, R., Kruizinga, B., and Vink, R., 2012. TROPOMI on the ESA Sentinel-5 Precursor: A GMES mission for global observations of the atmospheric composition for climate, air quality and ozone layer applications. Remote Sens. Environ. 120, 70–83.

Vilà-Guerau de Arellano, J., van Heerwaarden, C.C., van Stratum, B.J., van den Dries, K.,
2015. Atmospheric Boundary Layer: Integrating Chemistry and Land Interactions.
Cambridge University Press, New York, USA, p. 265.

Zander S. Venter, Kristin Aunan, Sourangsu Chowdhury, Jos Lelieveld, 2020. COVID-19 lockdowns cause global air pollution declines. Proceedings of the National Academy of Sciences 117 (32) 18984-18990. DOI: 10.1073/pnas.2006853117.

Zara, M., Boersma, K. F., Eskes, H., Denier van der Gon, H., Vilà-Guerau de Arellano, J., Krol, M., van der Swaluw, E., Schuch, W., Velders, G. J.M., 2021. Reductions in nitrogen oxides over the Netherlands between 2005 and 2018 observed from space and on the ground: Decreasing emissions and increasing O3 indicate changing NOx chemistry. Atmospheric Environment: X, 9, 1-12. https://doi.org/10.1016/j.aeaoa.2021.100104.

Ziemke, J. R., Oman, L. D., Strode, S. A., Douglass, A. R., Olsen, M. A., McPeters, R. D., Bhartia, P. K., Froidevaux, L., Labow, G. J., Witte, J. C., Thompson, A. M., Haffner, D. P., Kramarova, N. A., Frith, S. M., Huang, L.-K., Jaross, G. R., Seftor, C. J., Deland, M. T., and Taylor, S. L., 2019. Trends in global tropospheric ozone inferred from a composite record of TOMS/OMI/MLS/OMPS satellite measurements and the MERRA-2 GMI simulation. Atmos. Chem. Phys. 19, 3257–3269. https://doi.org/10.5194/acp-19-3257-2019.

https://doi.org/10.5194/acp-2022-110
Preprint. Discussion started: 7 April 2022

Zou, Y., Charlesworth, E., Yin, C.Q., Yan, X.L., Deng, X.J., Li, F., 2019. The weekday/weekend ozone differences induced by the emissions change during summer and autumn in Guangzhou, China. Atmospheric Environment 199, 114-126, ISSN 1352-2310. https://doi.org/10.1016/j.atmosenv.2018.11.019.

https://doi.org/10.5194/acp-2022-110
Preprint. Discussion started: 7 April 2022

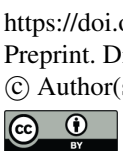

Atmospheric Chemistry and Physics Discussions

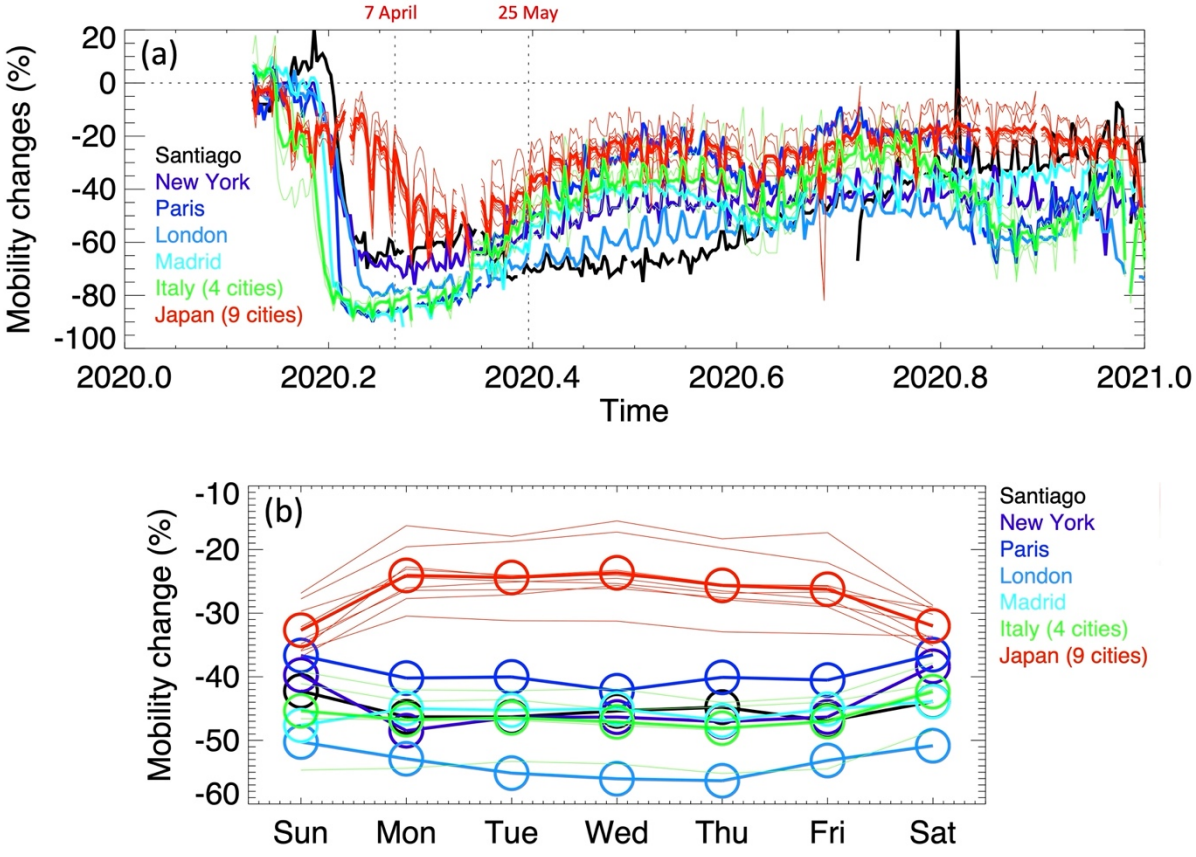

665 **Figure 1: Google mobility data for the place category Transit stations in 2020 compared to the pre-COVID period, for selected large metropolitan areas around the world strongly affected by the pandemic. For Japan and Italy, values were averaged (thick line) over 9 (Tokyo, Kanagawa, Saitama, Chiba, Kyoto, Nara, Osaka, Fukuoka, Nagasaki) and 4 (Milan, Rome, Naples and Turin) cities/prefectures (thin lines), respectively: (a) time series; (b) weekly changes. Holidays were removed.**

https://doi.org/10.5194/acp-2022-110
Preprint. Discussion started: 7 April 2022

Atmospheric Chemistry and Physics Discussions

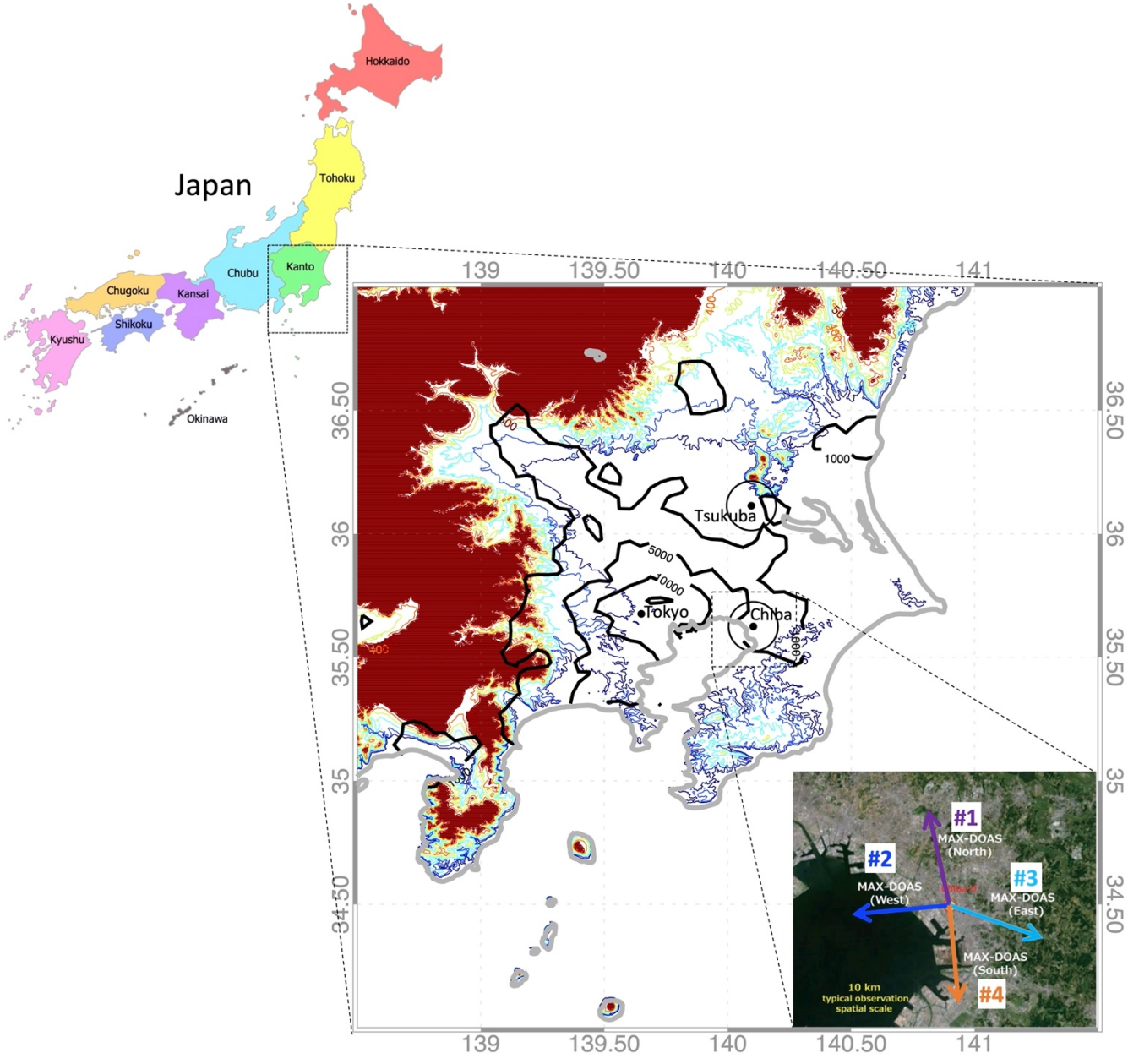

Figure 2: Main panel: Terrain map (meters above sea level, colored isolines; elevations > 0.5 km shaded dark red) from the General Bathymetric Chart of the Oceans (GEBCO) 2021 and population density (black isolines, people/km2) from the Gridded Population of the World, Version 4 (GPWv4). Circles highlight the average area sampled by the MAX-DOAS system (four azimuthal directions for Chiba, one direction for Tsukuba). The top inset shows the location of the investigated Kanto region in Japan and the bottom inset (© Google Maps 2019) shows the azimuthal pointing directions of the four MAX-DOAS systems deployed at Chiba University.

https://doi.org/10.5194/acp-2022-110
Preprint. Discussion started: 7 April 2022

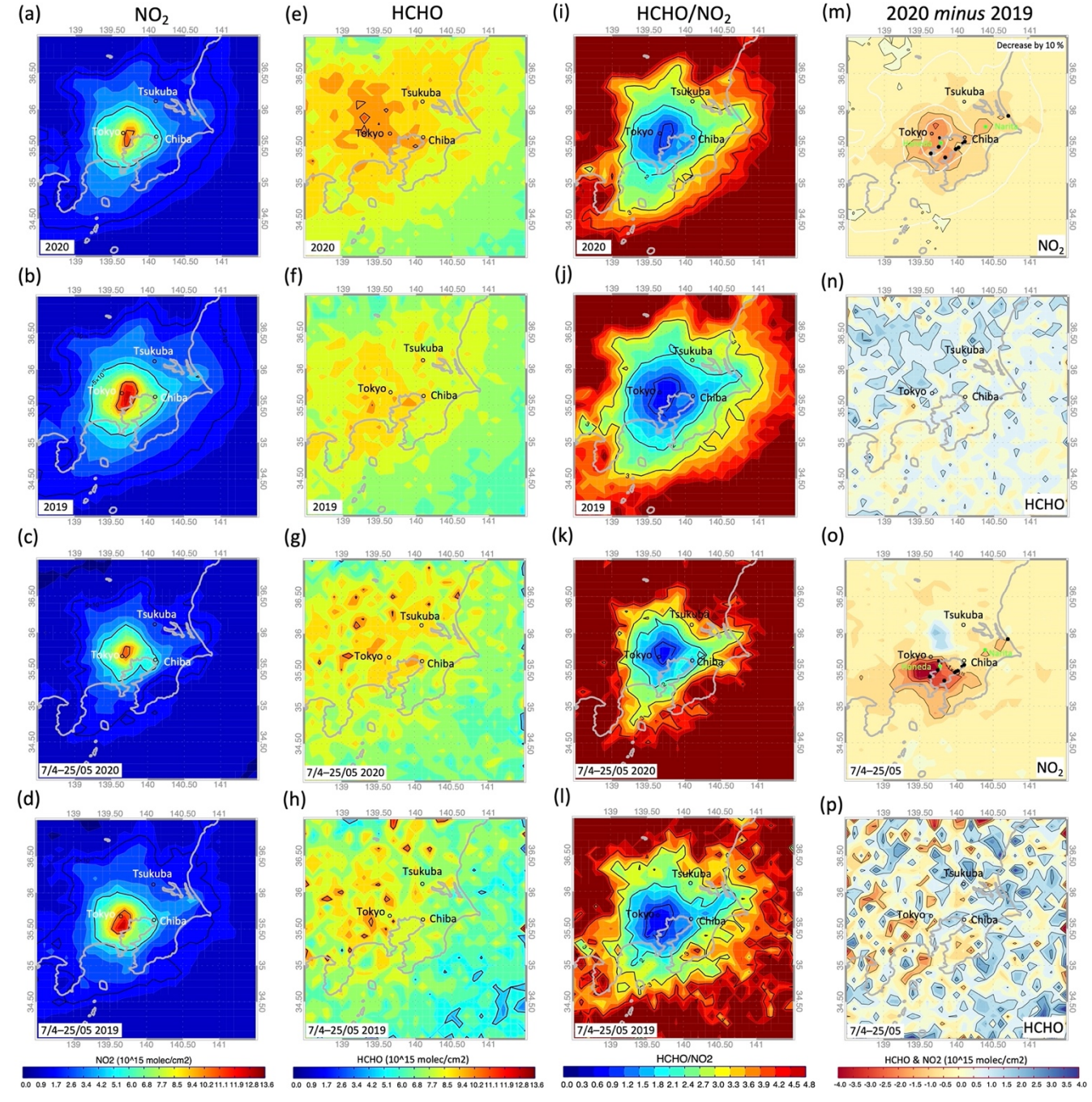

Figure 3: Top two panels: Spatial distribution of TROPOMI NO_2 (a,b), HCHO (e,f), and HCHO/NO_2 (i,j) in 2020 and 2019, as well as the 2020–2019 differences in NO_2 (m) and HCHO (n). Bottom two panels: Spatial distribution of TROPOMI observations is as described above but limited to 7 April–25 May (i.e., the state of emergency).

https://doi.org/10.5194/acp-2022-110
Preprint. Discussion started: 7 April 2022

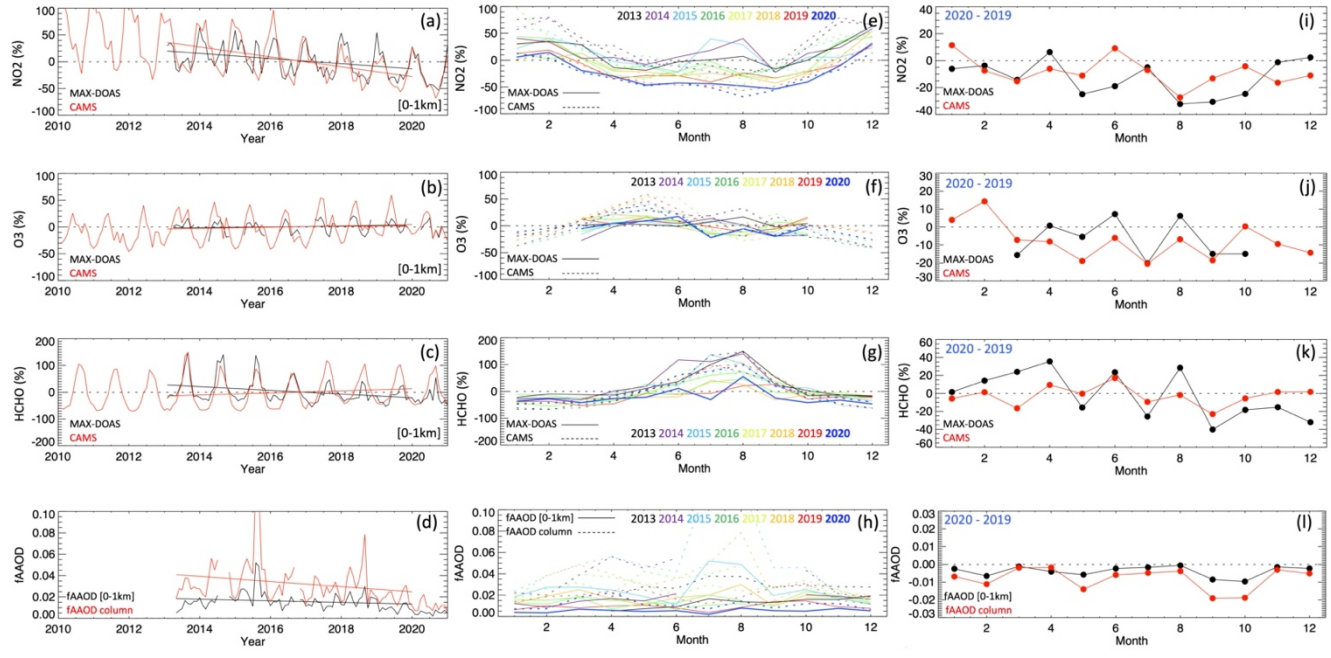

Figure 4: Left column: monthly time series of NO_2 (a), O_3 (b), and HCHO (c) partial column (< 1 km) as recorded by the MAX-DOAS system and estimated by CAMS at Chiba University. Central column: seasonal monthly changes in MAX-DOAS observations and CAMS estimates of NO_2 (e), O_3 (f) and HCHO (g). Right column: differences (2020 minus 2019) in MAX-DOAS observations and CAMS estimates for NO_2 (i), O_3 (j) and HCHO (k). Results are shown as percentage changes with respect to the 2013–2019 average (left and central panels) and 2019 (right panel). Bottom panel: changes as described above but for fine mode light-absorbing aerosols i.e., fAAOD and fAAOD (0–1 km).

https://doi.org/10.5194/acp-2022-110
Preprint. Discussion started: 7 April 2022

Atmospheric Chemistry and Physics Discussions

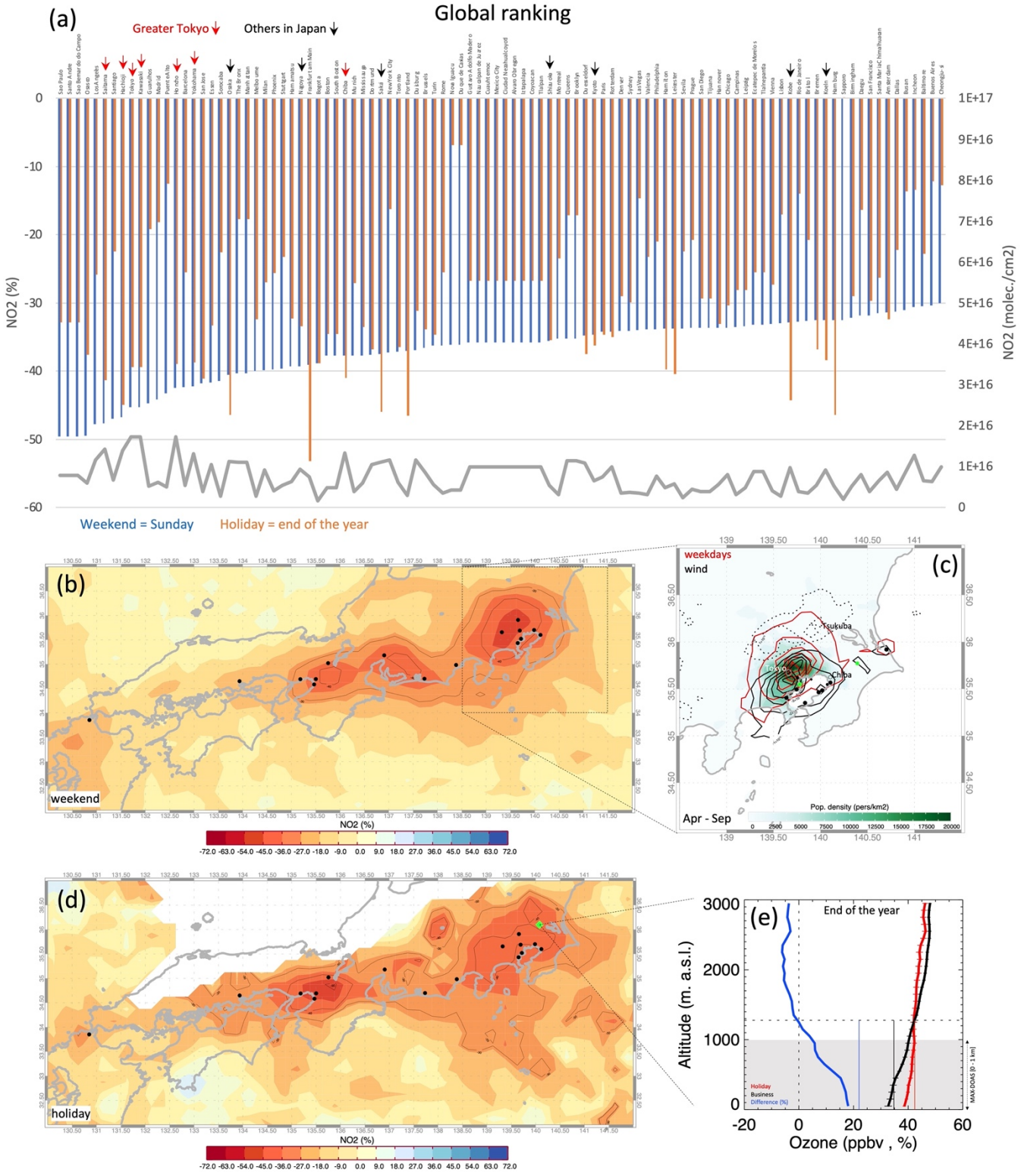

https://doi.org/10.5194/acp-2022-110
Preprint. Discussion started: 7 April 2022

Atmospheric Chemistry and Physics Discussions

Figure 5: Global ranking of the weekend effect (Sunday minus weekdays, blue) and holiday effect (end-of-year period minus business days, orange) for cities with a population greater than 0.5 million based on OMI NO_2 in 2005–2020. Only cities where changes were larger than 30% were shown. Opposite axis: mean NO_2 column (a). The spatial distribution of the weekend effect over Japan ((b), relative changes) and over the Kanto region ((c), absolute changes in red, limited to April–September; black points: power plants; green points: airports). Wind-related NO_2 changes (high minus low wind speed, black; depicted contour line values are as described for the weekend changes) and population density (filled contours, in green shades) are also plotted in (c). Spatial distribution of the holiday effect in NO_2 across Japan (d); the low number of OMI observations prevents determination of the difference along the coastline of the Japan Sea. Ozone profiles obtained from ozonesondes launched from Tateno (green point in (d)) during the end-of-year holiday period and business holidays in 2013–2020 (i.e., when MAX-DOAS data were available) are plotted along with box simulations (vertical lines) of the mean ozone concentration within the boundary layer (e). See Sect. 2 for further details.

https://doi.org/10.5194/acp-2022-110
Preprint. Discussion started: 7 April 2022

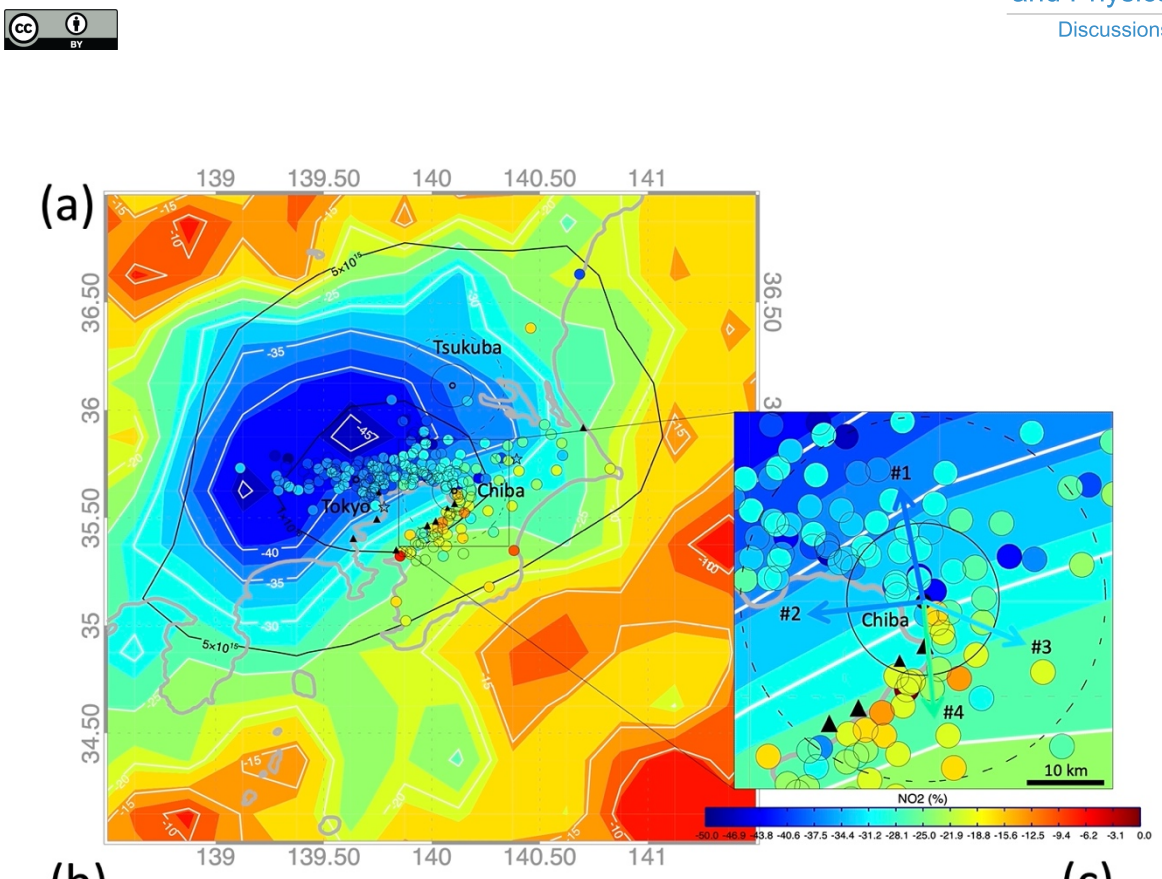

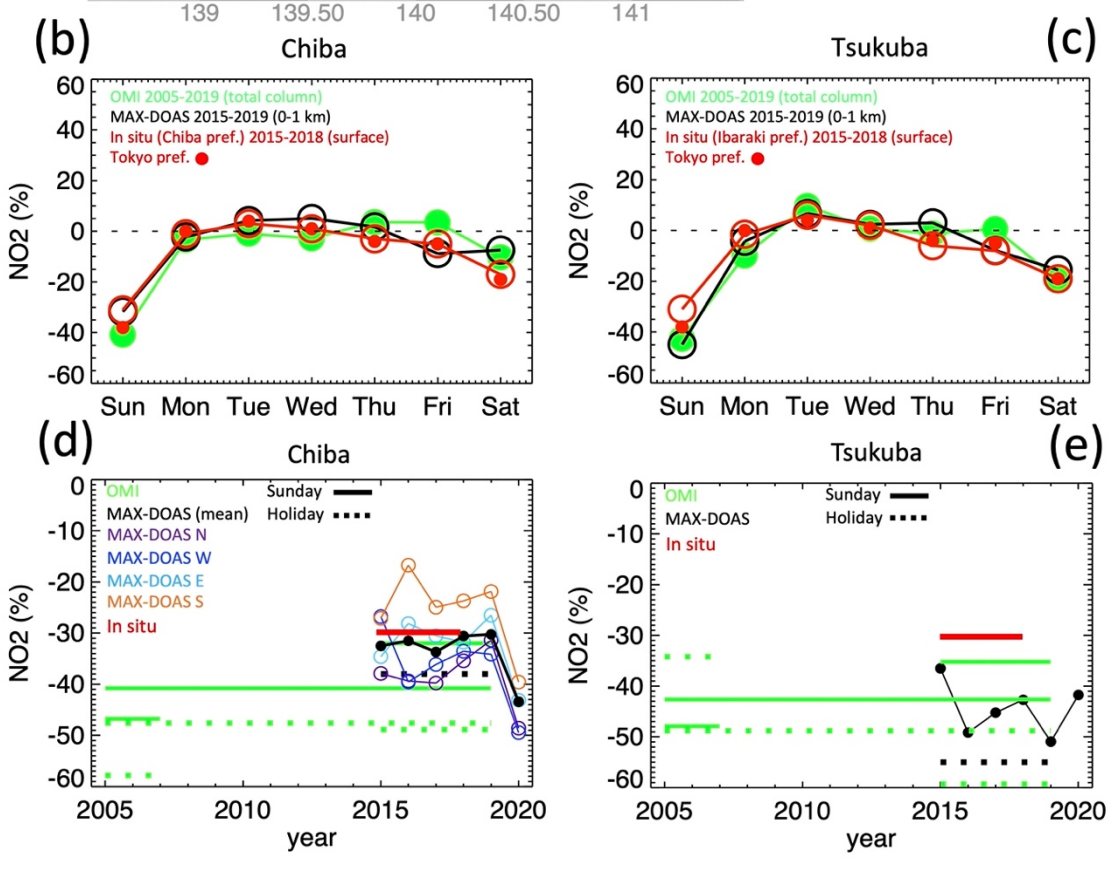

https://doi.org/10.5194/acp-2022-110
Preprint. Discussion started: 7 April 2022

Atmospheric Chemistry and Physics Discussions

Figure 6: Spatial distribution of the weekend effect (Sunday minus weekdays) based on OMI NO_2 tropospheric column (filled contours), MAX-DOAS partial column (< 1 km, colored arrows), and in situ NO2 observations (circles) over 2015–2018 ((a), main panel). Magnified view of the area around Chiba University (inset). NO_2 weekly cycle at Chiba and Tsukuba for the datasets noted above. In situ data were averaged across the prefecture (b,c). The weekend effect (on Sunday) and the holiday effect (at the end of the year) were averaged over different periods (as indicated by the horizontal lines) at Chiba and Tsukuba (d,e). MAX-DOAS NO_2 data are also plotted for each year and for each instrument at Chiba.

https://doi.org/10.5194/acp-2022-110
Preprint. Discussion started: 7 April 2022

Atmospheric Chemistry and Physics Discussions

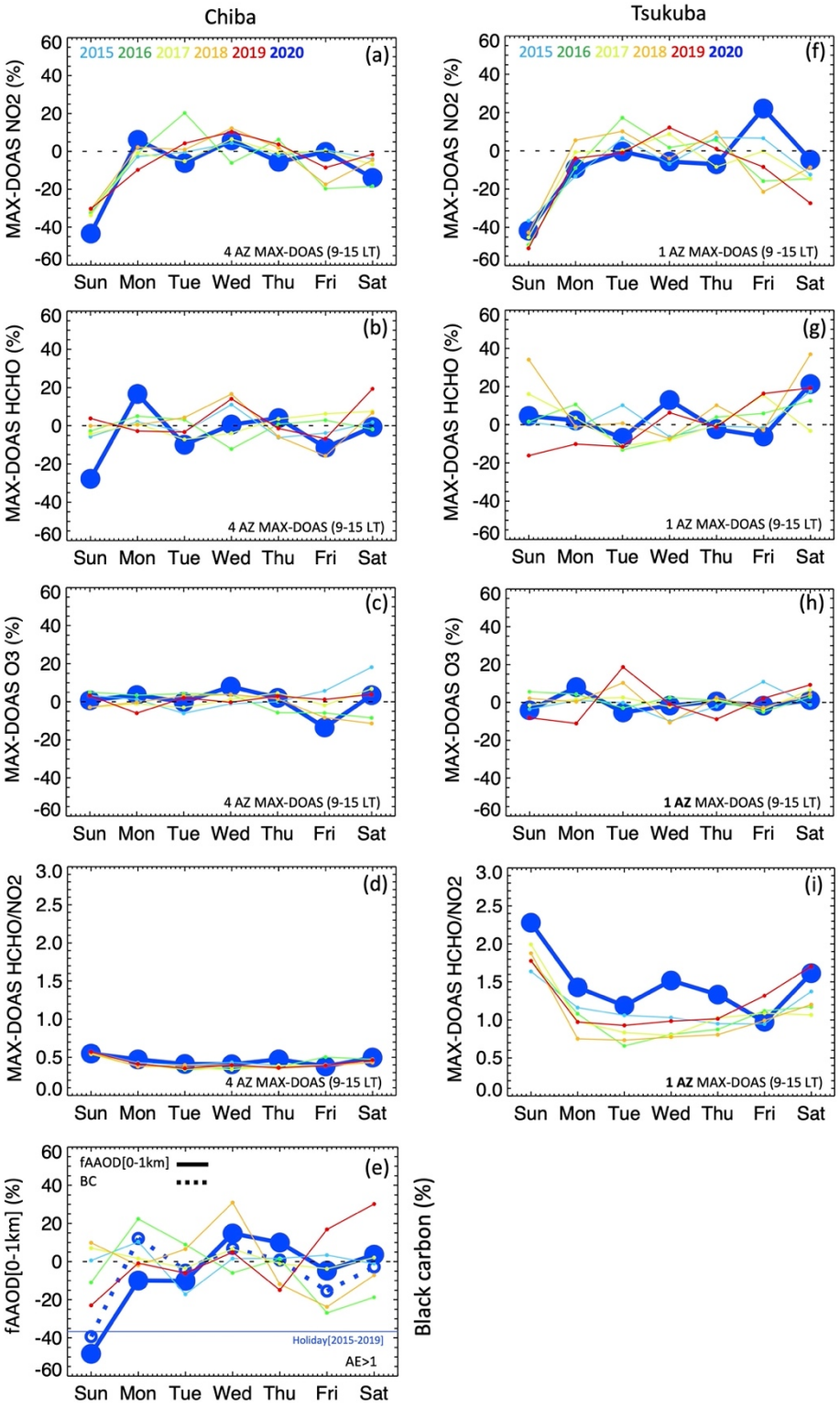

https://doi.org/10.5194/acp-2022-110
Preprint. Discussion started: 7 April 2022

Atmospheric Chemistry and Physics Discussions

Figure 7: Weekly changes in MAX-DOAS partial column (top to bottom) NO_2, HCHO, O_3, HCHO/NO_2, and fAAOD for Chiba (right) and Tsukuba (left) during 2015–2020. Only data with SZA < 50 were considered in the O_3 dataset; see text for details. Panel (e) includes the weekly cycle of surface BC concentrations. BC data were unavailable for Tsukuba.

https://doi.org/10.5194/acp-2022-110
Preprint. Discussion started: 7 April 2022

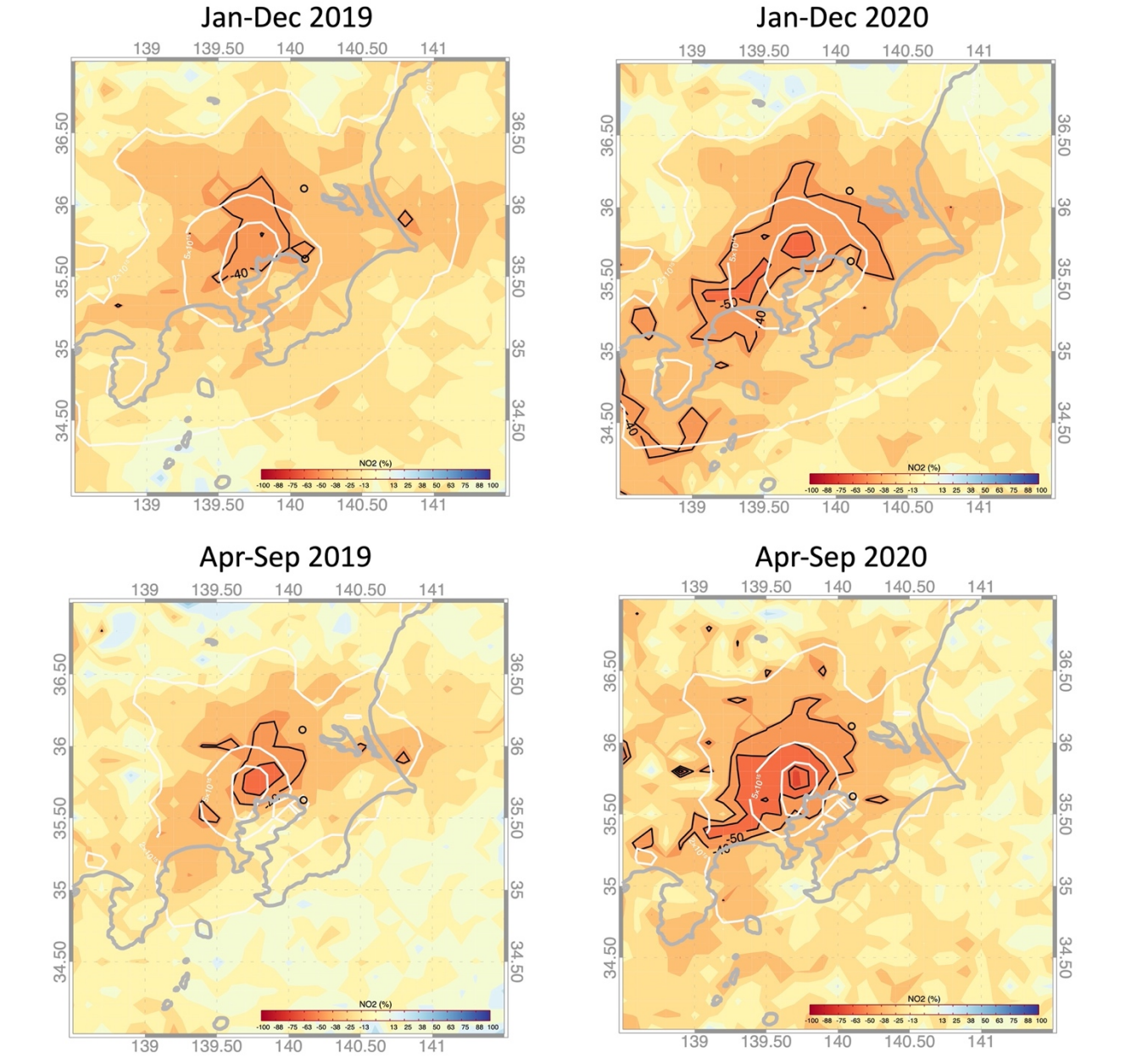

Figure 8: Spatial distribution of the TROPOMI NO_2 weekend effect (Sunday minus weekdays) in January to December 2019 (a), January to December 2020 (b), April to September 2019 (c), and April to September 2020 (d).

750